Shell-model study of the $M1$ dipole strength at low energy in the $A > 100$ nuclei

K. Sieja
IPHC, Université de Strasbourg, 23 Rue du Loess, 67037 Strasbourg, France
and CNRS, UMR7178, 67037 Strasbourg, France

(Received 30 July 2018; published 10 December 2018)

A low-energy enhancement of radiative strength functions was observed in experiment in several mass regions of nuclei, and it is believed to impact considerably the calculated neutron-capture rates. In the shell-model framework it was demonstrated to be possibly due to the magnetic dipole radiation. Up to now, the $M1$ deexcitation strength function was described within this framework in the mid-mass nuclei from the pf and pfg shells (e.g., ^{44}Sc, ^{50}Cr, ^{56,57,60,66,68}Fe, ^{59,60,70}Ni, $^{94–96}$Mo, ^{90}Zr), indicating systematically the presence of an up-bend at low energy. Therefore, the enhancement was accepted as a robust feature of the radiative decay. However, its exact magnitude and regions of emergence in the nuclear chart are still to be characterized in microscopic calculations. In this work, for the first time, the low-energy behavior of the radiative $M1$ strength in heavier nuclei, which can be described in the $g_{7/2}d_{5/2,3/2}s_{1/2}h_{11/2}$ shell, is investigated. The enhancement of the $M1$ deexcitation strength around $N = 80$ is confirmed, and is similar to that found previously in lighter nuclei. In contrast, no such up-bend is present on the proton drip line, in the deformed $N = Z = 54$ ^{108}Xe nucleus. From analysis of calculated magnetic dipole strengths the orbital nature of the observed enhancement is suggested. Photoemission and photoabsorption distributions on selected states are compared and the impact of different uncertainties in the theoretical treatment on the magnitude of $M1$ strengths at low photon energies is discussed.

DOI: 10.1103/PhysRevC.98.064312

I. INTRODUCTION

Radiative neutron capture plays a central role in the astrophysical models of nucleosynthesis and stellar evolution [1,2]. The determination of neutron capture cross sections for such applications requires theoretical predictions in hundreds of nuclei for which measurements are impossible. In this respect, nuclear structure theory models capable of describing statistical properties of nuclei, i.e., level densities and radiative strength functions, are required to provide reliable input for the calculations of reaction rates, usually described in the statistical approach of Ref. [3]. Commonly approximated by Lorentzian shapes, the experimentally determined dipole radiative strength functions reveal at low energies structure effects which cannot be captured by simple analytic formulas. For example, a low-energy enhancement of the radiative strength function was discovered via experiment in Ref. [4] and confirmed to exist in a large number of nuclei (see [5] for compilation of experimental results). The increased possibility of decay by low-energy γ rays is supposed to alter considerably the calculated neutron-capture cross sections.

This effect was explained in the nuclear shell-model approach due to the enhancement of magnetic dipole radiation between close-lying nuclear states of similar structures. Up to now, the studies of the magnetic strength at low energy within the shell model concerned selected mid-mass nuclei with $A = 40–96$ [6–11], confirming the presence of the low-energy spike in the majority of cases (the only exception so far being two pf-shell nuclei ^{48}Cr and ^{48}V; see Refs. [12,13]). The electric dipole strength has been studied using the shell model only in $A = 44–45$ nuclei [6], predicting a nonzero limit at $E_\gamma = 0$, but without structure effects comparable to the $M1$ case.

In a recent work [14] the new trends revealed in shell-model calculations were used to refine the low-energy part of deexcitation strength functions for further applications. For this purpose, the microscopic photoabsorption strength functions from the axially symmetric, deformed quasiparticle random-phase approximation (QRPA) calculations from Refs. [15,16] were supplemented by empirical zero-energy limits inspired by the shell model and adjusted to the available shell-model results and data. In addition to improving the agreement with data, this affected significantly the calculations of the average radiative widths and radiative neutron-capture cross sections, by factors up to a few hundreds in the most exotic nuclei. Of course, introducing the zero-energy limit determined in only several nuclides throughout the nuclear chart is a crude assumption. In the absence of fully microscopic models of the radiative decay which could be applied for all nuclei, more extensive shell-model calculations in various systems are thus valuable to improve such semimicroscopic treatment of the nuclear decays for applications, e.g., in nuclear astrophysics.

In this context, the present work proposes the first shell-model study of magnetic dipole deexcitation strength at low energy for heavier nuclei (preliminary results of this work for ^{134}Xe and ^{136}Ba were presented in Ref. [14]). First neutron-rich nuclei are examined: $N = 80$ isotones from Te ($Z = 52$) to Ce ($Z = 58$) and then tellurium isotopes, from ^{132}Te down to the stable ^{126}Te. They are described in the model space containing $g_{7/2}d_{5/2}d_{3/2}s_{1/2}h_{11/2}$ proton and neutron orbits with the GCN5082 interaction [17,18]. As the same model

space gives access to all nuclei between $Z = N = 50$ and $N = Z = 82$ closures, also a completely different system is examined, ^{108}Xe, which consists of a first study of the low-energy magnetic dipole on the proton drip line. The strong enhancement observed at the lowest γ-ray energies around $N = 80$ is found to be orbital driven, while the spin part of the magnetic operator is mostly enhanced in the spin-flip energy range. A gradual change of the magnitude of the up-bend from ^{134}Te towards ^{126}Te (increasing number of neutron holes) and towards ^{138}Ce (increasing number of active protons) is shown. A flat trend of the $M1$ strength is observed for the deformed ^{108}Xe that is in line with previous suggestions that the configuration mixing destroys the up-bend of the magnetic dipole strength. The differences between the deexcitation and photoabsorption strengths are discussed and deviations from the Brink-Axel hypothesis appear to be important for the 0^+ ground states of even-even nuclei.

The paper is organized as follows: the present shell-model framework is recalled in Sec. II. The results are collected in Sec. III. In Sec. III A a detailed analysis of proton/neutron and spin/orbital contributions to the calculated strengths is performed to characterize systematic effects that appear at low energy in nuclei below the $N = 82$ closure. The deformed ^{108}Xe is described in Sec. III B. The predictions of the deexcitation strength functions in studied systems are given in Sec. III C. Finally, in Sec. III D, the photoabsorption and deexcitation dipole strengths in selected cases are compared. Conclusions are given in Sec. IV.

II. SHELL-MODEL FRAMEWORK

In the present work the same model space and effective interaction are used which were employed in an earlier study of the mixed-symmetry (MS) states in the region [18]. The model space contains $g_{7/2}$, $d_{5/2}$, $d_{3/2}$, $s_{1/2}$, and $h_{11/2}$ orbitals for both protons and neutrons. The effective interaction, known as GCN5082, is an empirical fit based on the microscopically derived G-matrix interaction with the Bonn-C potential. The low lying states of all even-even and even-odd semimagic nuclei within the 50–82 valence space, all even-odd Sb isotopes and $N = 81$ isotones, as well as some known odd-odd nuclei around ^{132}Sn, were included in the fit. This allowed the authors of Ref. [17] to reproduce the experimental excitation energies of 320 states in 87 nuclei with a rms error of 110 keV [17].

The GCN5082 interaction was already explored in calculations of double-beta decays of ^{124}Sn, ^{128}Te, ^{130}Te, ^{136}Te, and ^{136}Xe [19–21] and in the investigations of the excitation spectra of ^{134}Xe up to 5 MeV, and an excellent agreement between theory and experiment was obtained for the levels of both parities [22]. As stated above, in the study of $N = 80$ isotones [18] special attention was paid to the electromagnetic transition rates and the structure of the excited 2^+ states, among which the mixed-symmetric ones are observed in this region. A good agreement was found with experiment for those as well as for the energy spectra of ^{132}Te, ^{134}Xe, ^{136}Ba and ^{138}Ce.

Due to the lack of the spin-orbit partners of the biggest orbits in the model space, i.e., the $g_{9/2}$ and $h_{9/2}$, renormalized g factors were necessary to reproduce the experimental magnetic moments. In Ref. [23] the measured g factors for Xe isotopes were reported and shell-model calculations were performed in the $gdsh$ valence space using a surface-delta interaction. The single-particle g factors were tuned in the calculations to reproduce the data: $g_l^\pi = 1.13$, $g_l^\nu = 0.02$, $g_s^\pi = 4.04$, and $g_s^\nu = -2.65$. These values were successfully employed to characterize the MS states in Ref. [18] and are thus kept the same in the present study.

The calculations of the present work are carried out using the shell-model code NATHAN [24]. A full diagonalization within the valence space is performed for $^{132-128}$Te, ^{134}Xe, and ^{136}Ba while for ^{138}Ce and ^{126}Te calculations are carried out up to seniority 8. The convergence pattern of the strength function with truncation is discussed.

To obtain averages of the reduced transition probabilities $B(M1)$ and radiative strength functions, 80 levels of each spin between $J = 0$ and $J = 7$ for both parities are computed. The number of transition matrix elements taken into account in the evaluation of average values is 66 920 for each parity.

III. RESULTS

A. $B(M1)$ strength at low transition energies in the $N = 80$ region

First, the results of the averaged $B(M1)$ strength as a function of transition energy E_γ for all calculated systems are discussed. The average $\langle B(M1)\rangle$ values are computed as a sum of all $B(M1)$ values per energy bin of 200 keV divided by the number of transitions within this bin. To get some more insight, the $B(M1)$ averages are also determined including only proton ($g_n = 0$) or neutron ($g_p = 0$) and only orbital ($g_s = 0$) or spin ($g_l = 0$) parts of the magnetic operator. The total averages are shown for $N = 80$ and for the Te chain in Fig. 1, separately for positive (π^+) and negative (π^-) parity states. Different contributions to those strengths are shown in Fig. 2 for one selected case, here ^{130}Te. It should be underlined, however, that the considerations made in this case hold for all nuclei discussed in this section as the calculated averages of transition probabilities share common features and are overall very similar, as seen in Fig. 1.

Several observations follow from Figs. 1 and 2:

(i) The low-energy enhancement of the $M1$ transition strength between both negative and positive parity states is present in all nuclei, though the slope of the $\langle B(M1)\rangle$ is steeper for negative parity. The magnitude of the enhancement is clearly decreasing with the number of active particles (holes) in the model space, i.e., from ^{132}Te to ^{138}Ce and from ^{132}Te to ^{126}Te.

(ii) The spike at the lowest photon energies is mostly due to the orbital part of the $M1$ operator, in both positive and negative parity states. This observation suggests that the low-energy enhancement of magnetic radiation shares a common origin with other orbital-driven phenomena observed in atomic nuclei, i.e., scissor modes in deformed nuclei or mixed-symmetry states

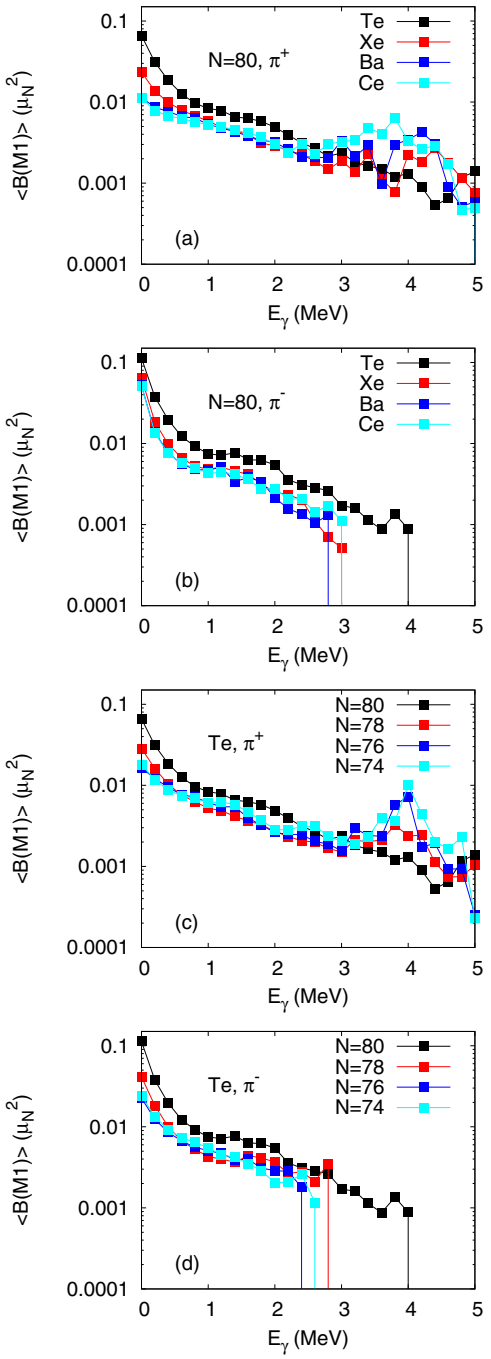

FIG. 1. Averaged $B(M1)$ strength as a function of transition energy in the $N = 80$ isotones and in the tellurium chain for positive and negative parity states.

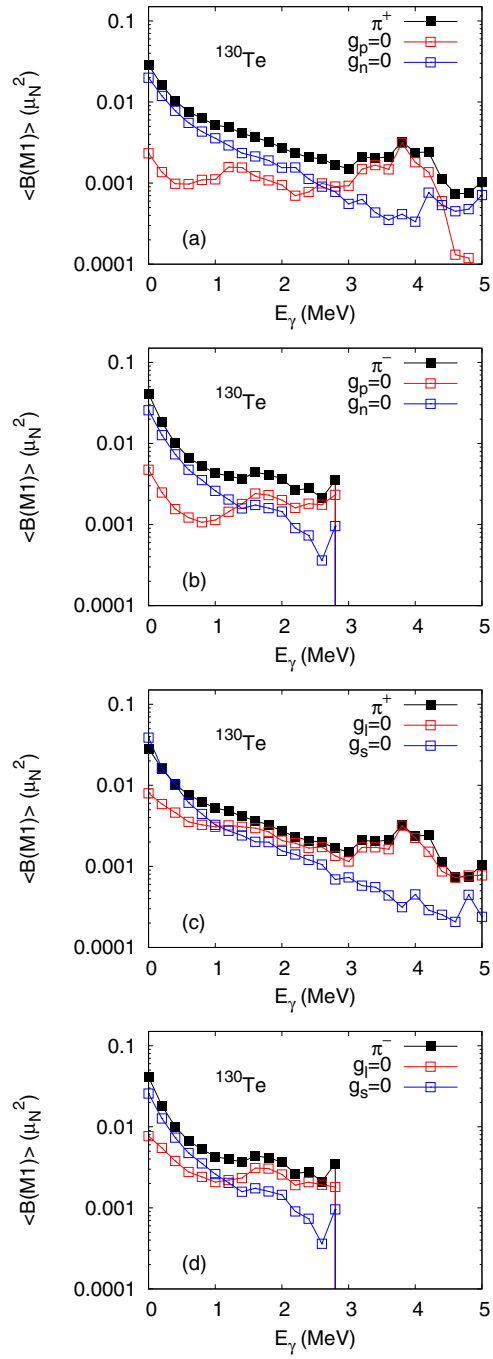

FIG. 2. Averaged $B(M1)$ strength as a function of transition energy for ^{130}Te. Contributions of proton ($g_n = 0$) and neutron ($g_n = 0$) or spin ($g_l = 0$) and orbital ($g_s = 0$) parts of the magnetic operator are distinguished for positive and negative parity states.

in vibrational ones (see, e.g., [25] for a review). The proton contribution dominates at low energy as the neutron $g_l \sim 0$.

(iii) The spin contribution to the calculated strengths also peaks at $E_\gamma = 0$ but has much a smaller amplitude than the orbital part. Besides, it exhibits structure effects between 1.5 and 2.5 MeV (π^- states) and 3.5 and 4.5 MeV (π^+ states). The increase of the decay probability in these two regions corresponds to the spin-flip transitions $d_{5/2} - d_{3/2}$.

To examine further the origin of the enhancement, the interpretations of the previously published works are revisited. In Ref. [9] it was proposed that the enhancement is related to the transitions between high-l single-particle orbitals and that these transitions will contribute to the low-energy $M1$ γ

strength in all nuclei. The contributions from diagonal and off-diagonal matrix elements were verified one by one in the selected case of ^{130}Te. The non-diagonal transitions ($d_{5/2} - d_{3/2}$) do not exhibit the low-energy enhancement for either positive or negative parity states, and only increase in the spin-flip region. As for the diagonal matrix elements, in negative parity states they are all enhanced at the lowest energy, irrespective of l. The largest contributions come from high-j orbits $d_{5/2}$, $g_{7/2}$, and $h_{11/2}$ while those from $s_{1/2}$ and $d_{3/2}$ are an order of magnitude smaller. In the positive parity states the enhancement is basically given by the contribution from $d_{5/2}$ - $d_{5/2}$ and $g_{7/2}$ - $g_{7/2}$ matrix elements, while the $h_{11/2}$ - $h_{11/2}$ part is negligible. The differences between the $h_{11/2}$ contribution to the positive and negative parities can be understood from the wave-functions' composition: The π^+ states do not contain active holes in the neutron $h_{11/2}$ orbital or particles in the proton one, which are necessary to create the π^- states. The total neutron $h_{11/2}$ occupation is $\sim$10 particles in the negative parity states and corresponds to the average of one-hole (11 particles) and three-hole (9 particles) configurations. It is also close to 10 in the positive parity states but corresponds to 10 particles coupled to $J = 0^+$. The occupancy of the proton $h_{11/2}$ orbital reaches 0.4 particle for higher energy negative-parity states while it does not exceed 0.1 for the positive-parity ones (and corresponds necessarily to scattering of a pair). Therefore, the contribution from high-l orbitals like $h_{11/2}$ depends on its occupation number and particular recoupling of involved particles. A strong enhancement is coming from a lower-l orbit, $d_{5/2}$, and a large difference of the magnitude of $d_{5/2}$ - $d_{5/2}$ and $d_{3/2}$ - $d_{3/2}$ matrix elements is observed; this indicates that the enhancement is j dependent rather than l dependent, and that a particular recoupling of protons and neutrons also appears necessary to produce strong $M1$ transitions.

Present results are more consistent with another interpretation, given in Ref. [7]. The authors postulated that the low-energy enhancement appears near closed shells, in nuclei where active protons and neutrons occupy high-j orbits near the Fermi surface, with magnetic moments adding up coherently. In the studied case, in negative parity states, one deals with high-j protons in $d_{5/2}$ and $g_{7/2}$ and active neutron holes in $h_{11/2}$; this is exactly what is needed for the shears bands generating magnetic rotation (see, e.g., [26] for a review), a phenomenon in which the high-j proton particles and neutron holes form current loops embedded in the near spherical mass distribution of a nucleus. The $\langle B(M1)\rangle$ from negative-parity states has a steeper slope and a larger amplitude than in positive-parity states, which recouple proton $d_{5/2}$, $g_{7/2}$ particles and neutron $d_{3/2}$, $s_{1/2}$ holes. Thus the magnetic rotation contributes strongly to the creation of the up-bend at low energy.

It should be noted that the $N = 80$ isotones are an example of nuclei with MS states found in their low-energy spectra. Such states appear in nuclei near closed shells where quadrupole vibrational oscillations dominate. They are not fully symmetric to the exchange of proton and neutron pairs (they have nonmaximum F spin in the interacting boson model notation) and are characterized by strong $M1$ transitions to the states which differ by one unit of F spin. In

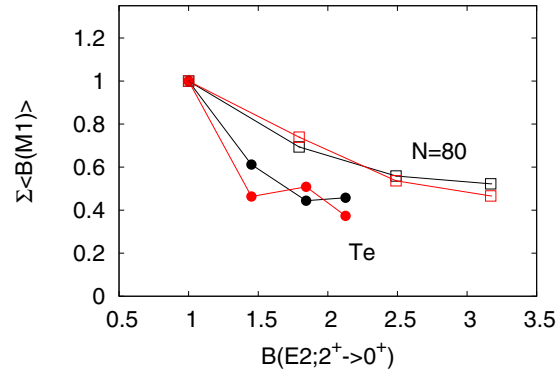

FIG. 3. Summed averaged deexcitation $M1$ strength (black) and its orbital part (red) versus the corresponding $B(E2; 2^+ \rightarrow 0^+)$ value for the $N = 80$ isotones (open symbols) and for the Te chain (filled symbols). The values are normalized to those in ^{132}Te. The lines are added to guide the eye.

Ref. [18] such states were described in the $N = 80$ isotonic chain within the shell model, concentrating only on the 2^+ states, but the experimental evidence exists also for the 1^+ and 3^+ mixed-symmetric states in this region. The strong $M1$ transitions from MS to symmetric states should thus contribute to the spike at $E_\gamma = 0.5$–1.0 MeV. It was also shown that $B(M1; 2^+_{MS} \rightarrow 2^+_1)$ is given essentially by the orbital part of the magnetic operator and that the MS states are more fragmented in cerium than in xenon, i.e., disappearing with the increasing number of active protons. All these features are replicated for the low-energy enhancement. This is also the case for the summed $\langle B(M1)\rangle$ strength as function of the γ transition energy: from evaluated sums from 0 to 4.5 MeV, the maximum value is obtained in ^{132}Te and it is about twice larger than in ^{126}Te and in ^{138}Ce. Additionally, in Fig. 3 the correlation is noted between the summed $\langle B(M1)\rangle$ strength (total and orbital) and the $B(E2; 2^+_1 \rightarrow 0^+)$ transition resulting from the shell model, which is the measure of the quadrupole collectivity. Apparently the total and orbital $\langle B(M1)\rangle$'s scale with the square of nuclear deformation. The tendency observed here in $N = 80$ isotones and Te isotopes, i.e., the decrease of the summed deexcitation $M1$ strength with increasing deformation, is exactly inverse to that of the integrated orbital strength from the ground state in deformed nuclei. As shown, e.g., in Fig. 15 of Ref. [25] in heavy barium isotopes, the summed orbital strength from the 0^+ state is linearly growing as a function of $B(E2; 0^+ \rightarrow 2^+_1)$ value.

Finally, in Ref. [18] the important role of pairing interactions in the creation of the mixed-symmetry states was pointed out. Recently, it was noted in Refs. [13,27] that the slope of the $\langle B(M1)\rangle$ is proportional to the $T = 1$ pairing matrix elements. The pairing interaction tends to purify wave functions, and favors the appearance of MS states and of the low-energy enhancement (see as well Fig. 2 of Ref. [12]). From this observation and the correlation presented in Fig. 3 it can be expected that the spike in the magnetic strength at low energy will disappear in systems with high seniority components dominating the wave functions, like the deformed nuclei addressed in the next section.

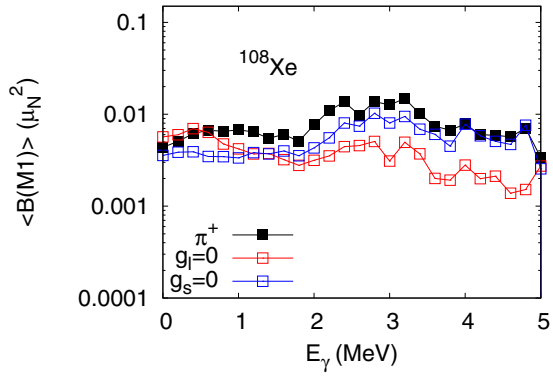

FIG. 4. Averaged $B(M1)$ strength obtained for ^{108}Xe.

B. $B(M1)$ strength at low transition energies on the $N = Z$ line

In Ref. [14], for the sake of astrophysics applications, the deexcitation strengths were modeled to include the low energy tail of the electric dipole and a spike in the magnetic dipole strength in all nuclei in the nuclear chart. The possible increase of the magnetic dipole at low photon energies appeared to affect considerably both the proton and the neutron capture cross sections, at both extremes of the valley of stability. The shell-model studies performed so far, like the experimental ones, considered mostly nuclei close to the stability line. Here one moves for the first time towards the proton drip line: this side of the nuclear chart poses a real challenge for the shell-model calculations. Many of the $N = Z$ nuclei are deformed, requiring large model spaces and thus huge computing efforts. In Ref. [28] such demanding calculations were performed to study deformation of light xenon isotopes, using the same model space and interaction as employed here. The experimentally known spectra of ^{110,112}Xe were reproduced accurately and the quadrupole properties were described, predicting the yet-unknown ^{108}Xe nucleus to be deformed in its ground state ($\beta = 0.16$) and to have a pronounced γ band.

Obtaining many excited states necessary to determine the radiative strength function in those systems is of course far more demanding from the computing point of view, thus only positive parity states in ^{108}Xe are treated here, excluding additionally the $h_{11/2}$ orbit from the model space. Its removal causes pairing renormalization, leading to a slight quenching of the spectrum and an increase of collectivity which is given by the pseudo-SU(3) model including $g_{7/2}, d_{5/2,3/2}, s_{1/2}$ orbits. This goes, however, in the desired direction, i.e., towards a weak-pairing regime which is interesting to explore. Otherwise, the same number of states (80) of each spin ($J_i = 0$–7) is considered, as in the calculations of heavier nuclei described in the previous section. The averaged dipole strength obtained this way in ^{108}Xe is shown in Fig. 4, together with the averages coming from spin and orbital parts of the $M1$ operator separately.

As anticipated, ^{108}Xe exhibits a different behavior of the dipole strength, confirming that the quadrupole collectivity destroys the spike in the $M1$ strength. Recall that no up-bend of the magnetic strength towards $E_\gamma = 0$ was theoretically predicted in another $N = Z$ nucleus, ^{48}Cr, which is an example of a deformed rotor in the pf shell [12]. It was later shown in Ref. [8] for neutron-rich, deformed iron nuclei that a part of the strength from the up-bend is shifted to the scissors resonance region. This mode, understood schematically as an oscillation between protons and neutrons similar to the movement of scissors, appears around 3 MeV in deformed nuclei and is microscopically related to the orbital part of the magnetic operator. The present strength in ^{108}Xe is indeed larger in the 2.5–3.5 MeV interval. The observed increase of the orbital strength in the same energy range is consistent with the scissors mode interpretation.

As in the case of ^{130}Te, also contributions from different single-particle $M1$ transitions in ^{108}Xe are examined. None of the diagonal matrix elements is really enhanced at low energies, irrespective of l number. They all have a flat trend, like the total averaged $B(M1)$'s, with the magnitude higher by one order for the high-j orbits ($g_{7/2}, d_{5/2}$) with respect to the low-j ones ($d_{3/2}$ and $s_{1/2}$). The nondiagonal part $d_{5/2}$ - $d_{3/2}$ is closer in magnitude to that of the high-j orbits and has a bump in the energy region 2–4 MeV. However, the contribution from the $g_{7/2}$ and $d_{5/2}$ levels also peaks in this energy range. The calculated states in ^{108}Xe have typically 1.6–1.8 particle in the $d_{5/2}$ orbital and 1.3–1.5 particle in the $g_{7/2}$ while the occupancies of the $d_{3/2}$ and $s_{1/2}$ are fractional. The $g_{7/2}$ occupancy is thus similar to that of protons in ^{130}Te studied in the previous paragraph but it does not suffice for the $g_{7/2}$ - $g_{7/2}$ contributions to peak at $E_\gamma = 0$. Therefore, the occupation of the high-$l(j)$ orbits itself is not a sufficient condition to produce a spike in the magnetic strength at low energy; the seniority content of wave functions and couplings of protons and neutrons play a role. The augmentation of the $M1$ at low energy should thus better develop in the proximity of closed shells. Nonetheless, the $M1$ contribution at $E_\gamma = 0$ is nonzero in the deformed cases and may still constitute a non-negligible correction to the electric dipole strength at low energy.

C. Derivation of the radiative dipole strength at low energy

To extract the radiative strength from the calculated shell-model transition probabilities, the following definition is used [29]:

$$f_{M1}(E_\gamma, E_i, J_i, \pi) = 16\pi/(9\hbar c)^3 \langle B(M1)\rangle \rho(E_i, J_i, \pi), \tag{1}$$

where $\rho_i(E_i, J_i, \pi)$ is the partial level density determined at a given initial excitation energy E_i. Thus the radiative strength depends on the behavior and magnitude of the $B(M1)$ distribution as well as on the adopted level density. The extraction of the radiative strength function in experiment within the so-called Oslo method [30] also requires the knowledge of level densities at two energies, which can be provided by experiment (discrete spectrum and neutron resonance spacings) or based on theory in the absence of the former. The shell model uses restricted valence spaces and only a limited number of states can be converged for practical reasons, which may lead to underestimation of the level densities already at intermediate energies. In the present calculations the densities start falling between 4.5 and 5 MeV. For this reason levels calculated above $E_{\rm exc} = 5$ MeV are

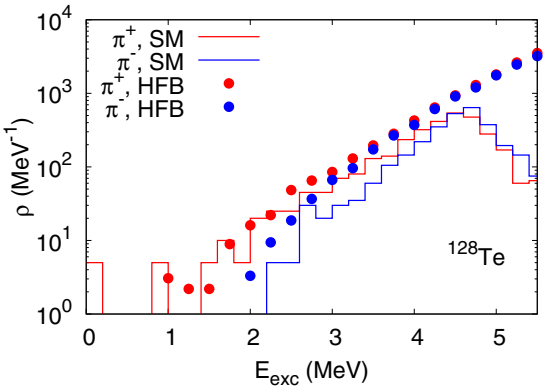

FIG. 5. Level densities from the shell model (steps) and HFB plus the combinatorial model (dots) for positive (red) and negative (blue) parity states with spins $J = 0$–7.

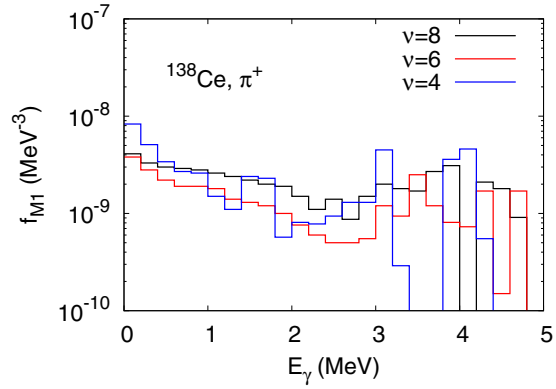

FIG. 7. Convergence of the f_{M1} for positive parity states in ^{138}Ce.

not included to extract the deexcitation strength functions. Further, as there is no experimental level density available for the systems studied here, shell-model results are compared to those from the Hartree-Fock-Bogoliubov plus combinatorial model available in RIPL-3 [31]. The comparison is shown in Fig. 5 in a selected nucleus, ^{128}Te, for positive and negative parity separately. Only levels with spins $J = 0$–7 are summed in the HFB model, as this is the spin range covered by the shell-model calculation. The HFB densities were shifted up by 0.75 MeV to obtain a better agreement with the known discrete spectra. The overall agreement between theoretical predictions is satisfying for the positive parity but the shell model predicts a larger parity asymmetry past 2.5 MeV and the HFB level densities are systematically larger for the π^- part.

To illustrate the impact of level densities chosen to extract the γ-strength function at low energy, the average $B(M1)$ values from the shell model are used and combined with either the level density from the shell model or with the HFB one to get the f_{M1} from Eq. (1). The result for the excitation energy range 0–4.5 MeV is shown in Fig. 6 in the case of ^{128}Te. Since above 2.5 MeV the level densities from the HFB model are

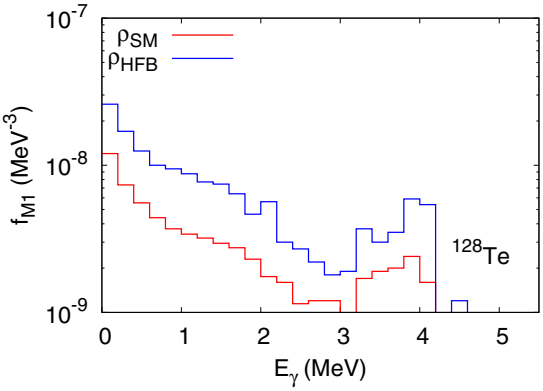

FIG. 6. Deexcitation strength function at low energy derived using the $M1$ strength from the shell model combined with shell-model or HFB level densities.

higher, especially for the negative parity states, the magnitude of f_{M1} is a factor 2.2 larger at $E_\gamma = 0$ and the total strength is shifted up in the whole considered energy range when the HFB model for the level densities is applied.

Another point to address in this context is the adopted truncation. In the case of ^{138}Ce and ^{126}Te the full space configuration mixing was not possible in the calculations, therefore a step-by-step evaluation of the strength function dependent on the truncation in the seniority (ν) scheme was performed. The ground state energies of the two nuclei converge at $\nu = 8$, with a difference of about 10 keV with respect to the $\nu = 10$ calculation. Going beyond seniority 8, however, would be too time consuming for the evaluation of hundreds of nuclear states necessary to extract the deexcitation strength function. The seniority 4, 6, and 8 calculations of f_{M1} for positive parity states are thus shown for ^{138}Ce in Fig. 7. The averaged $B(M1)$ values at $E_\gamma = 0$ are $0.06\mu_N^2$, $0.02\mu_N^2$, and $0.01\mu_N^2$ for $\nu = 4, 6, 8$, respectively. The corresponding numbers of π^+ levels in the energy interval 0–5 MeV are 100, 301, and 532. The f_{M1} for $\nu = 4$ is thus a result of compensation of too high averages and too low densities leading finally to a small (factor 2) difference at $E_\gamma = 0$, in spite of a factor 6 difference of $\langle B(M1)\rangle$ values. The amplitudes of the enhancement for $\nu = 6$ and $\nu = 8$ are nearly the same and the strengths have more similar shapes, though there is still a noticeable gap between them due to the lower level density in the more restricted calculation. Given the convergence pattern, one can, however, expect the $\nu = 8$ calculation would be close to the full-space diagonalization, if it was feasible.

In Fig. 8 I show the compilation of calculated strength functions. As in the case of the average $B(M1)$ values, the present shell model predicts in all nuclei near $N = 80$ very similar shapes of the deexcitation strength at low energy. The structure effects of f_{M1}'s are smoothened as compared to the averaged $B(M1)$'s but still present. There is a visible enhancement for both parities between $E_\gamma = 0$ and 1 MeV and the strength decreases by one order of magnitude after this interval, having a plateau between 1 and 2 MeV (from spin flip in π^- states) and increases slightly again around 3.5 MeV, due to the spin-flip transitions in π^+ states. The magnitude of the γ strength in the $E_\gamma = 0$ limit is decreasing with the growing

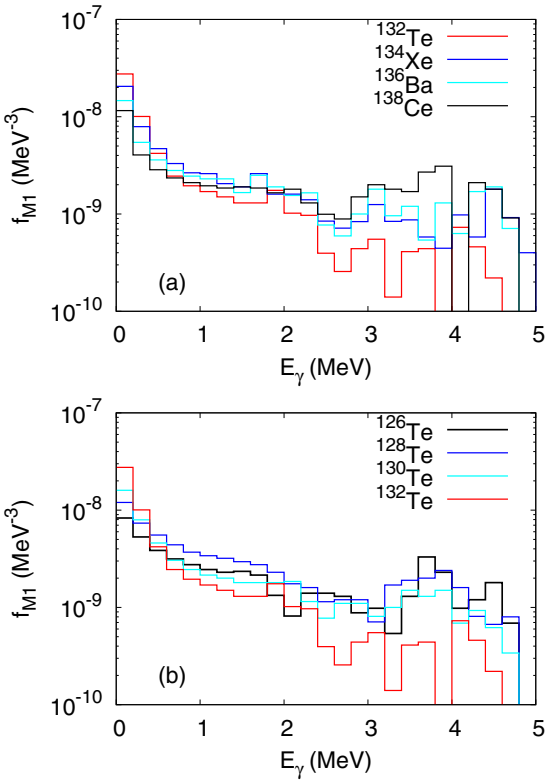

FIG. 8. Deexcitation strength functions obtained in the present work for $N = 80$ (upper panel) and for tellurium isotopes (lower panel).

number of active protons (i.e., from ^{132}Te towards ^{138}Ce for $N = 80$) and neutron holes (i.e., from ^{134}Te towards ^{126}Te).

The observed robustness of shell-model results from one region of nuclei to another indicates that the low-energy enhancement is a common feature of spherical and vibrational nuclei and that the $M1$ strength is not null at $E_\gamma = 0$ in the deformed nuclei. As such, a low-energy $M1$ correction should be included in semiempirical models of the radiative decay. On the other hand, its exact magnitude can be easily under/overestimated by a factor of several units by different uncertainties in the theoretical treatment, e.g., model space truncations and contributions from missing nuclear levels.

D. Photoabsorption versus radiative decay

It is now well accepted that the deexcitation function can differ from the photoabsorption on the ground state, especially at low photon energies. The shell model gives a possibility to obtain both strength functions in a fully microscopic way and using different numerical techniques. In this section a comparison of shell-model calculations of photoabsorption strength on individual states to the total deexcitation strength functions for selected cases is presented.

To begin, an example of averaged $B(M1)$ transitions between 1^+ states in ^{134}Xe is considered. Figure 9 shows the total deexcitation strength obtained by averaging all the transitions between all the calculated 1^+ states compared to the averaged transitions towards only the first, second, 15th, and

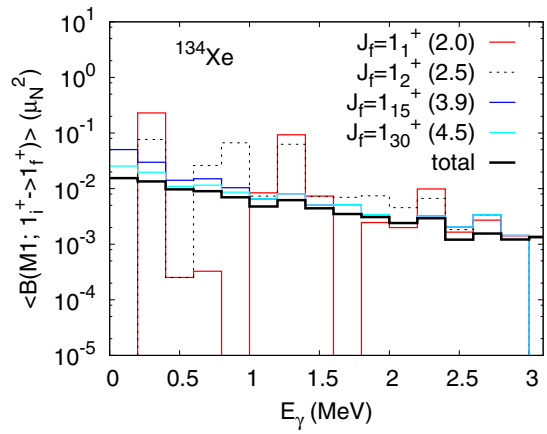

FIG. 9. Averaged $B(M1)$ strength to selected final states ($J_f = 1^+_{1,2,15,30}$) and including all final and initial 1^+ levels as function of transition energy (E_γ) in ^{134}Xe. Excitation energies of calculated states (in MeV) are given in parentheses.

30th 1^+ states (which is thus equivalent to the photoabsorption on those states). As can be seen, the higher the energy of the initial state, the closer the photoabsorption is to the total decay strength, clearly dominated by the photoemission from the high-lying states.

In the previous section it was explained how f_{M1} is extracted using the shell-model transitions probabilities and level densities. Converging hundreds of the lowest shell-model levels necessary for that may be time consuming, however: in the present study, typically 800 Lanczos iterations were needed to converge 80 states of one spin-parity with a precision of 0.001 MeV, which means in total 12 800 iterations to get the f_{M1} value in one nucleus. Applying such a method in large valence spaces required for computations of deformed, open-shell nuclei and of $E1$ transitions becomes too time consuming to allow for more systematic shell-model predictions of deexcitation strengths in different regions of the nuclear chart. Therefore, the best approximation to the total decay strength was looked for in an even-even nucleus, using the Lanczos strength function (LSF) method proposed by Whitehead [32], which permits an efficient computation of transition probabilities and their distribution (see, e.g., [24] for an overview). To obtain the photoabsorption strength function, 100 Lanczos iterations were carried out and the peaked-fence structure of calculated $B(M1)$'s was smoothed with a Lorentz distribution

$$L(x, x_0, \Gamma) = \frac{1}{\pi} \frac{\gamma}{(x - x_0)^2 + \gamma^2}, \tag{2}$$

with $\gamma = \Gamma/2 = 0.5$ MeV.

The results are shown in Fig. 10 for the spherical nucleus ^{134}Xe and in Fig. 11 for the deformed nucleus ^{108}Xe. In ^{134}Xe the following initial levels are considered: the ground state 0^+, the first 2^+ state calculated at 886 keV (experimental value 847 keV), and the first 6^+ state calculated at an energy of 2088 keV, in very good agreement with the experimental value of 2136 keV. They are compared to the total

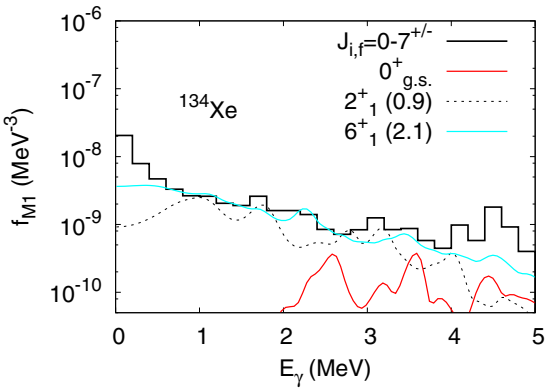

FIG. 10. Photoabsorption versus deexcitation strength in ^{134}Xe resulting from shell-model calculations. Excitations energies of the calculated states (in MeV) are given in parentheses.

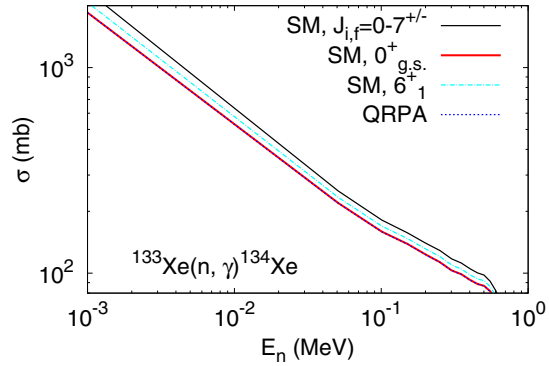

FIG. 12. ^{133}Xe$(n,\gamma)^{134}$Xe cross section as a function of the energy of incident neutrons obtained with QRPA $E1$ and $M1$ strengths and with the QRPA $M1$ strength with a low-energy part replaced by a shell-model prediction. See text for more details.

deexcitation strength function obtained as described in the previous section.

As one can see, the photoabsorption strength distributions on the 2^+_1 and 6^+_1 states are nonzero in the $E_\gamma = 0$ limit, in contrast to that of the 0^+ ground state. One should note that due to the Brink-Axel hypothesis the photoabsorption cross section should be independent of the initial state. While this is more or less fulfilled for the $M1$ absorption on excited states, it is not true for the ground state. The large gap in the spectra of ^{134}Xe (and any other even-even nucleus), where the first 1^+ state is located above 2 MeV, causes the absence of strength at the lowest γ energies.

The structure effects visible in the 2^+ distribution can be traced back to the transitions between the symmetric and mixed-symmetric states appearing at low excitation energies in ^{134}Xe. The higher the excitation energy of the initial state, the smoother is the strength function and the closer it is to the total deexcitation f_{M1}. From Fig. 9 it could be anticipated that it would be preferable to consider the photoabsorption on a higher excited level than on the first ones. For both excited states, however, the zero-energy limit is still too low when compared to the deexcitation strength, causing a visible mismatch in the 0–0.8 MeV energy range.

The same type of calculation in ^{108}Xe is shown in Fig. 11. To describe the photoabsorption in, the ground state and excited 4^+_1 and 7^+_1 states are considered. The deexcitation

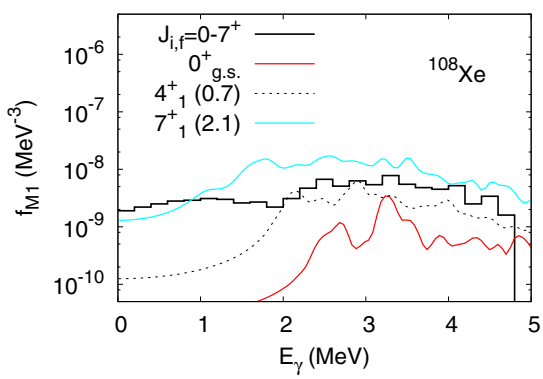

FIG. 11. The same as in Fig. 10 but for the ^{108}Xe nucleus.

strength is not enhanced for the lowest photon energies but has a small and constant value of the order 10^9. In the averaged $B(M1)$ distribution a small increase between 2 and 4 MeV can be noticed in Fig. 4, which is interpreted as a scissor mode. Convoluted with the level density, it is still visible in the trend of the total f_{M1}. Concerning photoabsorption, the same features as in ^{134}Xe are noted. For the ground state the photoabsorption does not match the photoemission from highly excited states below $E_\gamma = 2$–2.5 MeV. The photoresponse of a higher lying state (7^+_1) is a better approximation to the deexcitation strength function.

Finally, the impact of the form and magnitude of the $M1$ strength on the ^{133}Xe$(n,\gamma)^{134}$Xe cross section is examined. The TALYS code [33–35] is used and the QRPA-Gogny microscopic $E1$ and $M1$ strengths employed (the same as in Ref. [14]). In the latter the lowest energy part (up to 3.5 MeV) is replaced by the shell-model predictions for different states. The result is shown in Fig. 12 with the original QRPA $M1$ strength, with the shell-model photoabsorption on the ground and on the 6^+ states, as well as with the total decay strength. There is no difference if the $0^+_{g.s.}$ strength from the shell model or from the QRPA is used. This is obvious since both approaches give in this case no $M1$ strength below ∼2 MeV. The total deexcitation strength leads to the largest cross section, while with the 6^+ strength distribution the result falls in between the remaining ones. Though the differences in cross sections obtained here are negligible (factor 1.3) it might not be necessarily true for all nuclei. A similar calculation was done previously in iron nuclei in Ref. [36]. Using the microscopic shell-model strength of the first excited 2^+ instead of that of the ground state in the Hauser-Feshbach calculations led to an increase of the ^{67}Fe$(n,\gamma)^{68}$Fe cross section by a factor of 2. This difference will be more important in neutron-rich nuclei where a very limited number of states is available below the neutron separation energy.

Based on results from Figs. 10–12 it can be concluded that the photoabsorption on an excited state in an even-even nucleus captures the main features of the deexcitation strength and is a better approximation to describe the decay of the compound nucleus than the ground state photoresponse, usually studied in theoretical approaches. Since it can be obtained at a

moderate computing effort using the LSF method, it provides a reasonable alternative to calculations of averages of large numbers of shell-model transition probabilities [Eq. (1)] in cases where the latter are impossible.

IV. SUMMARY AND CONCLUSIONS

For the first time, shell-model calculations of the low-energy magnetic dipole deexcitation strength functions were performed in nuclei with masses $A > 100$. It was shown that the augmentation of the $M1$ strength at low energy is a common feature of nuclei around the $N = 82$ shell closure and that its magnitude can be related to the degree of the collectivity of the nuclear system. Consequently, the calculations in the $N = Z$ nucleus ^{108}Xe reveal the absence of a low-energy up-bend in the $M1$ deexcitation strength function. It is further demonstrated that the lowest-energy enhancement, like the scissors mode resonance, is dominated by the orbital part of the magnetic operator.

The absorption on the ground state and on an excited state are shown to be unequal due to the large gap between the 0^+ ground state and the first 1^+ in even-even nuclei. Consequently, the deexcitation strength is better approximated by photoabsorption on a higher-lying excited state, and the Brink-Axel hypothesis is well fulfilled at higher excitation energies. Computing the photoabsorption on an excited state using the LSF method may be the way of estimating the $M1/E1$ strengths at low energy at a moderate computing effort, and it offers a possibility of accessing the cases where converging hundreds of lowest shell-model states is too time consuming.

The current findings are a valuable contribution to the theoretical studies of the γ-strength functions. Together with earlier shell-model results, they provide a coherent picture of enhancement effects emerging near closed shells and moving to the scissor mode region with increasing deformation. The robustness of shell-model predictions in this and previously studied regions of nuclei indicates that semiempirical and phenomenological models of γ decay need to take into account the changes of the $M1$ strength function at low energy related to the nuclear shape. While the shell-model trends are preserved in various calculations, the exact magnitude of f_{M1} at $E_\gamma = 0$ is subject to theoretical uncertainties, which are estimated to be several units in the $E_\gamma = 0$ limit.

The next important step in determining microscopically the structure effects appearing in strength functions at low energy will be to study neutron-rich, exotic nuclei and to examine the role of the dipole radiation in the neutron capture in the limit of low level densities. Such studies are currently in progress.

Note added. Recently a new shell-model study was noticed [37] which presents systematic calculations of $M1$ strength at low energy in the sd-shell and pfg-shell nuclei. The results presented in [37] indicate a substantial decrease of the $M1$ strength at low energy in open-shell, deformed nuclei with respect to those near closed shells, which is in line with observations from the present work.

ACKNOWLEDGMENT

I am indebted to Stéphane Hilaire for help with the TALYS code and stimulating discussions.

[1] B. Burbidge, G. Burbidge, A. Fowler, and F. Hoyle, Rev. Mod. Phys. **29**, 547 (1957).
[2] M. Arnould, S. Goriely, and K. Takahashi, Phys. Rep. **450**, 97 (2007).
[3] H. Feshbach, C. Porter, and V. Weisskopf, Phys. Rev. **96**, 448 (1954).
[4] A. Voinov *et al.*, Phys. Rev. Lett. **93**, 142504 (2004).
[5] http://www.mn.uio.no/fysikk/
[6] K. Sieja, Phys. Rev. Lett. **119**, 052502 (2017).
[7] R. Schwengner, S. Frauendorf, and A. C. Larsen, Phys. Rev. Lett. **111**, 232504 (2013).
[8] R. Schwengner, S. Frauendorf, and B. A. Brown, Phys. Rev. Lett. **118**, 092502 (2017).
[9] B. A. Brown and A. C. Larsen, Phys. Rev. Lett. **113**, 252502 (2014).
[10] A. C. Larsen, J. E. Midtbø, M. Guttormsen, T. Renstrøm, S. N. Liddick, A. Spyrou, S. Karampagia, B. A. Brown, O. Achakovskiy, S. Kamerdzhiev *et al.*, Phys. Rev. C **97**, 054329 (2018).
[11] T. Renstrom *et al.*, arXiv:1804.08086.
[12] K. Sieja, EPJ Web Conf. **146**, 05004 (2017).
[13] S. Karampagia, B. A. Brown, and V. Zelevinsky, Phys. Rev. C **95**, 024322 (2017).
[14] S. Goriely, S. Hilaire, S. Péru, and K. Sieja, Phys. Rev. C **98**, 014327 (2018).
[15] M. Martini, S. Péru, S. Hilaire, S. Goriely, and F. Lechaftois, Phys. Rev. C **94**, 014304 (2016).
[16] S. Goriely, S. Hilaire, S. Péru, M. Martini, I. Deloncle, and F. Lechaftois, Phys. Rev. C **94**, 044306 (2016).
[17] A. Gniady, E. Caurier, F. Nowacki, and A. Poves (unpublished).
[18] K. Sieja, G. Martinez-Pinedo, L. Coquard, and N. Pietralla, Phys. Rev. C **80**, 054311 (2009).
[19] E. Caurier, J. Menendez, F. Nowacki, and A. Poves, Phys. Rev. Lett. **100**, 052503 (2008).
[20] E. Caurier, F. Nowacki, and A. Poves, Eur. Phys. J. **36**, 195 (2008).
[21] J. Menendez, A. Poves, E. Caurier, and F. Nowacki, Nucl. Phys. A **818**, 139 (2009).
[22] A. Shrivastava, M. Caamaño, M. Rejmund, A. Navin, F. Rejmund, K. H. Schmidt, A. Lemasson, C. Schmitt, L. Gaudefroy, K. Sieja *et al.*, Phys. Rev. C **80**, 051305 (2009).
[23] G. Jakob, N. Benczer-Koller, G. Kumbartzki, J. Holden, T. J. Mertzimekis, K.-H. Speidel, R. Ernst, A. E. Stuchbery, A. Pakou, P. Maier-Komor *et al.*, Phys. Rev. C **65**, 024316 (2002).
[24] E. Caurier, G. Martinez-Pinedo, F. Nowacki, A. Poves, and A. P. Zuker, Rev. Mod. Phys. **77**, 427 (2005).
[25] K. Heyde, P. von Neumann-Cosel, and A. Richter, Rev. Mod. Phys. **82**, 2365 (2010).

[26] S. Frauendorf, Rev. Mod. Phys. **73**, 463 (2001).
[27] S. Karampagia, B. A. Brown, and V. Zelevinsky, J. Phys.: Conf. Ser. **966**, 012031 (2018).
[28] E. Caurier, F. Nowacki, A. Poves, and K. Sieja, Phys. Rev. C **82**, 064304 (2010).
[29] G. Bartholomew, E. Earle, A. Ferguson, J. Knowles, and M. Lone, Adv. Nucl. Phys. **7**, 229 (1973).
[30] A. Schiller, L. Bergholt, M. Guttormsen, E. Melby, J. Rekstad, and S. Siem, Nucl. Instrum. Methods Phys. Res., Sect. A **447**, 498 (2000).
[31] S. Goriely, S. Hilaire, and A. J. Koning, Phys. Rev. C **78**, 064307 (2008).
[32] R. Whitehead, *Moment Methods in Many Fermion Systems*, edited by B. J. Dalton, S. M. Grimes, J. D. Vary, and S. A. Willimans (Plenum, New York, 1980).
[33] http://www.talys.eu
[34] A. Koning, S. Hilaire, and M. Duijvestijn, in *Proceedings of the International Conference on Nuclear Data for Science and Technology, ND 2007*, Nice, France, April 22–27, 2007 (EDP Sciences, Les Ulis, France, 2008), p. 058.
[35] A. Koning and D. Rochman, Nucl. Data Sheets **113**, 12 (2012).
[36] H. Loens *et al.*, Eur. Phys. J. **48**, 34 (2012).
[37] J. Midtbo *et al.*, arXiv:1807.04036.